Full Length Article

Experimental investigation on entrainment in two-phase free jets

Christian Hotz [a],[*], Manuel Haas [a], Simon Wachter [a], Sabine Fleck [a], Thomas Kolb [a],[b]

[a] Karlsruhe Institute of Technology (KIT), Institute for Technical Chemistry (ITC), Gasification Technology Department, Hermann-von-Helmholtz-Platz 1, 76344 Eggenstein-Leopoldshafen, Germany
[b] Karlsruhe Institute of Technology (KIT), Engler-Bunte-Institute, Division of Fuel Technology (EBI ceb), Engler-Bunte-Ring 1, 76131 Karlsruhe, Germany

ARTICLE INFO

ABSTRACT

In the present research, the influence of atomization on the mixing ratio, representing entrainment in the gas phase of a two-phase free jet, is investigated at ambient conditions. The local mixing ratio is determined from the tracer gas (helium) concentration in the gas phase. Radial profiles of the mixing ratio are measured at several axial distances for 3 different nozzles applying 5 different gas-to-liquid ratios (GLR) for the two-phase free jet as well as a single-phase free jet. Common characteristics between the two-phase free jet and the single-phase free jet have been found. The mixing ratio of the two-phase free jet can be modeled using a semi-empirical approach for single-phase free jets from literature. The experimental data is used to determine the empirical parameters of the two-phase free jet model for the simulation of the flame structure in an entrained flow gasifier from Hotz et al., 2021 (https://doi.org/10.1016/j.fuel.2021.121392) (Hotz et al., 2021). The experimental data of the mixing ratio is available on Mendeley data as supplementary material of the present research (https://doi.org/10.17632/t66f8swg6w.1) (Hotz, 2022).

1. Introduction

1.1. Motivation and background

Single-phase free jets are subject to many investigations carried out both experimentally [3–8] and numerically [9–11]. Using a single-phase free jet approach, reacting free jets, e.g. gas flames, can be described. Two-phase free jets include a continuous phase (e.g. gas) and a disperse phase (e.g. droplets). Experimental investigations on two-phase free jets are often focused on the size, velocity and distribution of the disperse phase, created during the atomization, under ambient conditions [12–17]. Numerical investigations on two-phase free jets using CFD simulation are also available [18–20]. Reacting two-phase free jets are found in many physical and thermo-chemical processes, e.g., entrained flow gasification. In an entrained-flow gasifier, the liquid fuel is atomized at the burner nozzle by the gasification medium. Typical gas-to-liquid ratios (GLR) for entrained flow gasifier are GLR < 1 as the oxygen content in the gasification agent is high to reach high reaction temperature and the equivalence ratio (ER) is ER < 1 [21–24]. The reactor wall of the gasifier encloses the two-phase jet, thus an outer recirculation zone is formed. Synthesis gas, recirculating from downstream of the reactor, is entrained into the jet, emerging from the nozzle,

and reacts with the gasification medium. An overview of the subprocesses during entrained flow gasification is given in [25]. Entrained-flow gasification has been simulated using a computational fluid dynamic (CFD) model [26].

A confined free jet can be described in good approximation as a free jet, up to the center of the recirculation eddy [27–30]. With the concept of the equivalent nozzle diameter, free jet equations can also be applied to reacting free jets, e.g. gas flames [31]. In the two-phase free jet model in [1], a free jet approach, derived from a single-phase free jet, is used to simulate the flame structure of an entrained flow gasifier. The flame is modeled as a superposition of a reacting free jet and a fuel spray, which is evaporating combustible components and interacts with the reacting free jet. In [1], the momentum flux of the gas phase is several orders of magnitude higher than the momentum flux of the liquid phase. Therefore, the two-phase free jet is considered as gas free jet emerging from an annular gap superimposed by the liquid phase. Velocity and concentration patterns are calculated with two-phase balance equations. As the two-phase free jet model is derived from a single-phase free jet, the difference between the gas phase of a two-phase free jet compared to a single-phase free jet is of interest.

Experimental data regarding the gas phase of a two-phase free jet is scarcely available in literature (e.g. [32–35]). In the present research,

---

* Corresponding author.
  E-mail address: christian.hotz@partner.kit.edu (C. Hotz).

the influence of the liquid phase on the mixing ratio in the gas phase of the two-phase free jet is investigated under ambient conditions without confinement of the jet. The experimental data is provided as supplementary material [2].

1.2. Free jet theory

The two-phase free jet investigated in the present study consists of the droplets as the disperse phase and the atomization medium as the continuous phase, which is diluted by gas entrained into the jet. The driving force in the two-phase free jet is the high momentum flow of the atomization medium as the liquid phase emerges the nozzle at low velocity. Fig. 1 displays a single-phase free jet emerging from a nozzle. The outlet velocity u_0 is constant across the nozzle orifice with the diameter d_0. The jet is in contact with quiescent gas in the surrounding environment. Due to the velocity gradient, the surrounding gas is entrained into the jet. The overall momentum flow of the jet is conserved [5]. The moving mass of the jet is increased and its velocity decreased. On the jet axis, the velocity of the jet is not affected by entrainment up to a distance of approximately 4 d_0, which represents the end of the core region. In this region, the flow pattern depends e.g. on nozzle design, Reynolds number and jet medium [36–39]. After a transition region, the similarity region begins at a distance of 6–8 d_0 [7,40,41]. In this region, radial velocity profiles show self-similarity, i.e. the profiles at different axial distances, normalized by the ratio of axial distance and the nozzle diameter collapse in good approximation on a single line [3,5,6]. Furthermore, the radial velocity profiles concur with a Gaussian function [7,42–47].

The atomization medium emerging from the nozzle is diluted with gas entrained from the surrounding environment. The mixing ratio is used to describe the entrainment and it is defined as the local mass ratio of the gas originating from the nozzle $m_{g,0}$ and the gas entrained into the jet $m_{g,1}$ (Eq. (1)). The radial position η and the axial position ζ are formulated as non-dimensional parameters (Eq. (2) - (3)), with the radial position r, the axial position z, the virtual jet origin z_0 (see Fig. 1) and the equivalent nozzle diameter d_{eq} (Eq. (4)). The equivalent nozzle diameter is introduced by Thring & Newby [29]. As given in Eq. (4), d_{eq} is the nozzle diameter of the hypothetical free jet with the momentum flow rate $\dot{I}_0$ and the mass flow rate $\dot{m}_{g,0}$ of the emerging jet and gas density of the surrounding environment ρ_1. With the concept of the equivalent nozzle diameter, Eq. (5) and (6) can be also applied to free jets from non-round nozzles and free jets with density gradients to the surrounding. The radial profiles of the mixing ratio also concur with a

Gaussian function. On the centerline of the jet ($\eta = 0$), the mixing ratio decays proportionally to $1/\zeta$ (see Eq. (5)). For the position of the virtual jet origin z_0 (see Fig. 1), values between $z_0 = -2 \bullet d_{eq}$ and $z_0 = +4 \bullet d_{eq}$ can be found in literature [41]. For the constant B_C of the free jet, values in the range of 4.3–5.3 have been reported in literature [9,38,40,41,48,50,51].

Günther et al. [48] developed a semi-empirical model to describe the mixing ratio of the single-phase free jet in the self-similar region (Eq. (6)). The model is based on radial Gaussian profiles. The conservation of the momentum, mass, and energy of the flow emerging from the nozzle, as well as the self-similarity of the jet, are assumed. The parameter for the exchange of momentum c_i is derived from experimental values at the centerline. For single-phase free jets, Kremer [52] determined c_i as a constant equal to 0.07. The turbulent Schmidt number Sc_t in Eq. (6) is set to 0.75 [48].

Definition of the mixing ratio:

$$X(\zeta, \eta) = \frac{m_0(\zeta, \eta)}{m_0(\zeta, \eta) + m_1(\zeta, \eta)} \tag{1}$$

Normalized radial position:

$$\eta = \frac{r}{z - z_0} \tag{2}$$

Normalized axial position:

$$\zeta = \frac{z - z_0}{d_{eq}} \tag{3}$$

Equivalent nozzle diameter:

$$d_{eq} = \frac{2 \bullet \dot{m}_{g,0}}{\sqrt{\dot{I}_0 \bullet \pi \bullet \rho_1}} \tag{4}$$

Centerline mixing ratio:

$$X(\eta = 0) = B_C \bullet \frac{1}{\zeta} \tag{5}$$

Mixing ratio in the self-similar region of a single-phase free jet:

$$X(\zeta, \eta) = \frac{Sc_t}{2 \bullet c_i} \bullet \frac{1}{\zeta} \bullet \exp\left(-\left(\frac{2 \bullet Sc_t - 1}{2 \bullet c_i^2} \right) \bullet \eta^2 \right) \tag{6}$$

1.3. Two-phase free jets

The driving force of the two-phase free jet is the momentum of the atomization medium, which accelerates the droplets, and which is
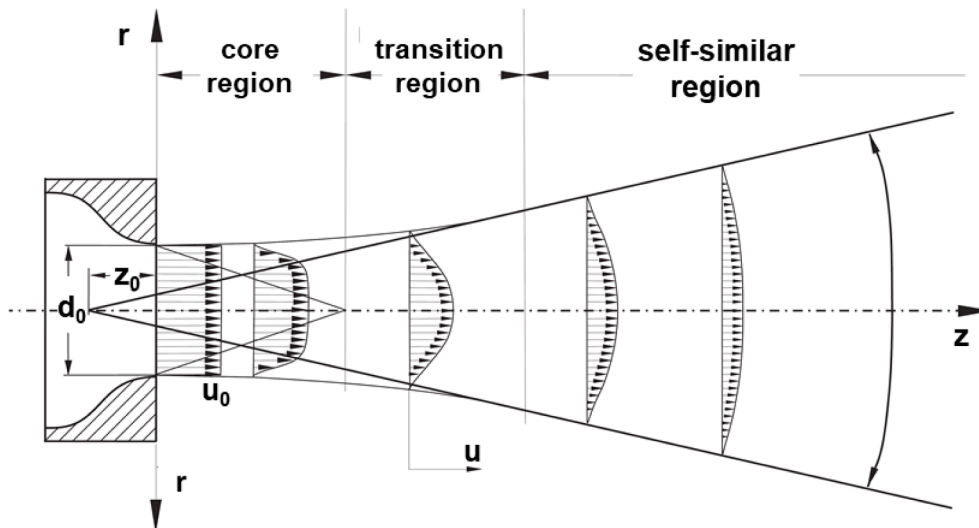
Fig. 1. Radial velocity profiles in the core, transition and self-similar region of a single phase free jet emerging from a round nozzle [48,49].

therefore, in turn, decelerated. The atomization medium is also decelerated by gas from the surrounding environment entrained into the jet. As the gas phase velocity is below the velocity of the droplets, the momentum is transferred from the droplets to the gas phase. The density of the droplets is 3 orders of magnitude higher than the density of the gas phase. Therefore, the droplets are centers of high inertia. As the moving mass of the gas increases significantly in the axial direction from the nozzle and the mass of the droplets remains constant, the influence of the droplets decreases with increasing axial distance from the nozzle.

The droplets may also influence the turbulence structure of the gas phase and therefore the entrainment of the jet. Large droplets may enhance the turbulence level of the gas phase, due to the vortex shedding phenomena. Small droplets may decrease the turbulence of the gas phase due to damping effects by the inertia of the droplets [33,34,53–55].

Two-phase free jets have received little attention in the literature, which is also reflected in the lack of systematic measurements [56]. Due to the limited experimental data available, only fragmented descriptions of single effects are to be found in the literature, rather than a comprehensive description of the two-phase free jet. The present work provides experimental data for the validation of computational models in order to gain a more complete understanding of the two-phase free jet.

2. Methods

2.1. Experimental set-up

The two-phase free jet experiments are carried out in the Atmospheric Spray Test Rig (ATMO) under ambient conditions. The experimental set-up is shown in Fig. 2. Water emerging from the central orifice of an external-mixing twin-fluid nozzle is atomized using pressurized air. The water droplets and the atomization medium (pressurized air), as well as air entrained from the surrounding environment, form the two-phase free jet. The two-phase free jet is collected in a topless container. The container is equipped with a honeycomb structure in order to prevent droplets from recirculating and re-entraining into the jet.

The pressurized air is enriched with a small amount ($y_{He,0} = 0.05$ mol/mole $= 0.007$ kg/kg) of helium as a tracer gas in order to

distinguish the atomization medium and air entrained into the jet. The admixture of helium leads to a small density gradient between the air from the nozzle ρ_0 and the environment ρ_1 ($\rho_0/\rho_1 = 0.994$), which is considered in the equivalent nozzle diameter (see Eq. (4)). The local mixing ratio X, which was defined in Eq. (1), is determined from Eq. (7), with the mass concentration of helium in the atomization medium at the nozzle $y_{He,0}$ and local mass concentration of helium $y_{He}(\zeta,\eta)$. The helium mass concentration is derived from the gas concentration, which is measured with a micro gas chromatograph (μGC) system (Agilent-490 Micro GC/MS5A). The tracer gas is selected, as the μGC systems features a high sensitivity for the detection of helium, due to the high thermal conductivity of the gas. The accuracy of the concentration measurement is in the range of 2 % of $y_{He,0}$, due to the helium-air admixture used for the calibration of the μGC.

$$X(\zeta,\eta) = \frac{y_{He}(\zeta,\eta)}{y_{He,0}} \tag{7}$$

The twin-fluid lance is movable vertically and the gas probe horizontally, thus concentration measurements can be performed at different radial and axial distance from the nozzle. The local tracer gas concentration $y_{He}(\zeta,\eta)$ is measured at 17 radial positions in the range of $\eta = \pm0.2$ and additionally at $\eta = \pm0.3$. Radial profiles are measured at 5 axial distances in the range of $10 \leq \zeta \leq 50$.

In order to investigate the influence of the atomization process on the gas phase of the free jet, experiments are performed using 3 nozzles, which differ in terms of the size of the annular gas gap (see Table 1). The

Table 1
Nozzle dimensions and operating conditions of the gas phase for the 3 different nozzles applied for the two-phase free jet experiments.

Nozzle	1	2	3
d_l/mm	2.0	2.0	2.0
d_g/mm	7.2	6.6	4.2
d_{eq}/mm	6.6	5.8	3.0
$\dot{m}_{g,0}$/kg/h	10.0	8.9	4.6
$u_{g,0}$/m/s	72	80	156
$\dot{I}_{g,0}$/N	0.2	0.2	0.2
Re_g/1000	20.4	19.4	13.1
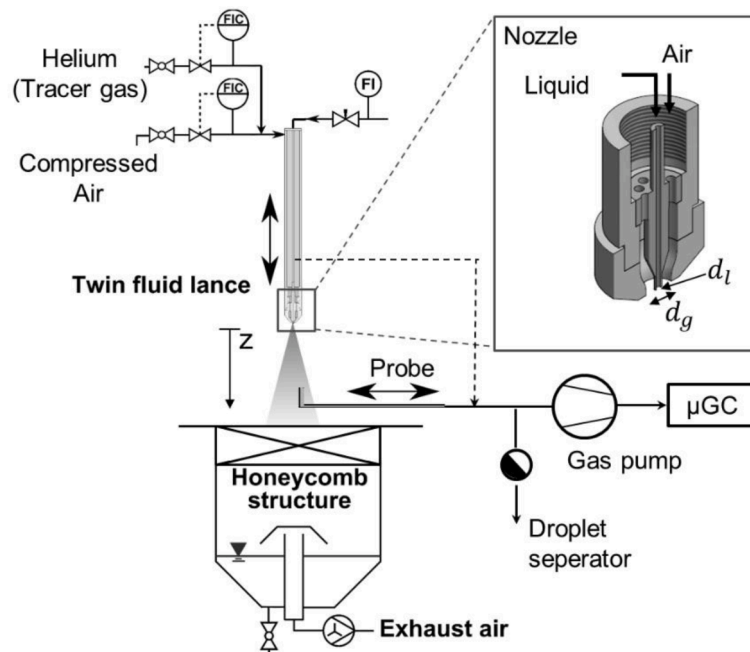
Fig. 2. Experimental set-up of the Atmospheric Spray Test Rig (ATMO) for measuring entrainment in a two-phase free jet [1].

diameter of the central orifice for the liquid is constant for all nozzles. In order to maintain comparability among the experiments conducted, the momentum flow of the gas phase, which is the driving force of the free jet, is kept constant in all experiments (see Table 1). Therefore, the gas outlet velocity at the nozzle is adapted to the area of the annular gap A_g for the 3 different nozzles. The momentum flow of the liquid phase does not contribute significantly to the overall momentum, as the momentum flow of the liquid phase is two orders of magnitude smaller than the momentum flow of the gas phase. The momentum flow of the gas phase $\dot{I}_{g,0}$ is defined in Eq. (8).

Following [57], the primary jet breakup can be classified, according to the operating conditions, into different atomization regimes. The operating condition of nozzles 1 and 2 lead to atomization in Fiber-type breakup with pulsating sub-mode. Operating conditions of nozzles 1 and 2 are typical for gasification experiments conducted in the REGA gasifier [25]. In the pulsating sub-mode, the high momentum of the gas-phase amplifies interfacial waves on the liquid jet known as Kelvin-Helmholtz instability [58,59]. The gas phase draws ligaments off the primary liquid jet. In between the interfacial waves, large eddies are formed in the gas phase, which pushes the liquid ligament and also the liquid primary jet in radial direction, which is described as flapping [60]. Subsequently, the liquid disintegrated into smaller droplets to minimize the liquid surface known as Rayleigh-Plateau instability. The radial acceleration of the liquid disintegrating to droplets, leading to a wide spray angle [61] (see also Fig. 7). Primary breakup of the liquid jet emerging from nozzle 3 is in the Fiber-type regime with super-pulsating sub-mode, where no flapping of the primary liquid jet occurs. In super-pulsating sub-mode, the liquid primary jet is atomized instantly at the nozzle orifice. The interfacial waves are not formed on the liquid primary jet and thus, no large gas eddies are present, which would push the liquid in radial direction. Super-pulsating sub-mode results typically in smaller droplets, due to higher aerodynamic forces compared to pulsating-sub-mode [57]. Fiber-Type breakup with pulsating and super-pulsating sub-mode is described in more detail in [62].

The influence of the liquid mass flow on the two-phase free jet is investigated for all 3 nozzles. As the momentum of the atomization medium is kept constant for all of the experiments, the liquid mass flow $\dot{m}_{l,0}$ is set according to the gas-to-liquid ratio (GLR) (see Eq. (9) varied from 0.5 to 1.5 with an increment of 0.25.

Momentum flow of the gas phase at the nozzle:

$$\dot{I}_{g,0} = u_{g,0}^2 \bullet \rho_{g,0} \bullet A_g \tag{8}$$

Gas-to-liquid ratio at the nozzle:

$$GLR = \frac{\dot{m}_{g,0}}{\dot{m}_{l,0}} \tag{9}$$

2.2. Data processing

The radial profiles of the mixing ratio $X(\zeta, \eta)$ are determined from the measured values of $y_{He}(\zeta, \eta)$ with Eq. (7). Each radial profile of X is fitted to a Gaussian function of the type shown in Eq. (10) using the non-linear least-square solver lsqnonlin of Matlab® [63,64]. The coefficients in Eq. (10) represent the peak value of the profile (a), the central position of the profile (b) and the parameter, which represents the width (c) of the Gaussian curve. The radial position of the experimental data is shifted in radial direction using coefficient b, and so the peak of the profile is located on the axis. The quality of the fit is evaluated using the standard deviation given in Eq. (11) with the deviation ΔX of each value obtained from the experiment and Eq. (10) with fitted parameters a, b and c.

$$X = a \ast \exp\left(-\left(\frac{\frac{r}{z} - b}{c}\right)^2\right) \tag{10}$$

$$\sigma = \sqrt{\frac{1}{n-1} \ast \sum_{i=1}^{n} \Delta X(\zeta, \eta)^2} \tag{11}$$

2.3. Determination of the parameter for the exchange of momentum c_i

The two-phase free jet model (2Ph-FJM) presented in [1], is based on the semi-empirical model of [48] given in Eq. (6). The parameter for the exchange of momentum c_i in Eq. (6) is determined from the two-phase free experiments for 3 different nozzles (see Table 1). c_i is obtained by minimizing the difference of the measured values of X, and X calculated from Eq. (6) using the non-linear least-square solver lsqnonlin of Matlab® [63,64]. In Eq. (6), the turbulent Schmidt number Sc_t is set to 0.75 [48]. ζ and η are the axial and radial position. The quality of the fit is again evaluated, using the standard deviation given in Eq. (11), with the deviation ΔX of the each value obtained from the experiment and Eq. (6) with fitted parameter c_i.

3. Results and discussion

Measurements are performed using the 3 different nozzles, each at 5 axial and 19 radial positions for 5 different GLR (two-phase free jet) and air (single-phase free jet). Each radial profile of X is fitted to a Gaussian function of the type shown in Eq. (10). Fig. 3 shows the radial profile of nozzle 1 using GLR = 0.5 at the axial position z = 65 mm and the respective Gaussian function as example data.

The standard deviation of the measured values and the fitted Gaussian functions is determined from Eq. (11) with the total number of measurements $n = 1425$ in the two-phase free jet. The standard deviation is calculated to be equal to $\sigma = 0.0053$. The small value of σ indicates, that the radial profiles of the mixing ratio in the gas phase of the two-phase jet can be represented by Gaussian functions to a good degree of approximation. For single-phase free jets, Gaussian functions are found for the concentration (mixing ratio) and velocity by many authors [5,7,42,43,65]. The investigation presented here confirms the characteristic to also be valid for the two-phase free jet.
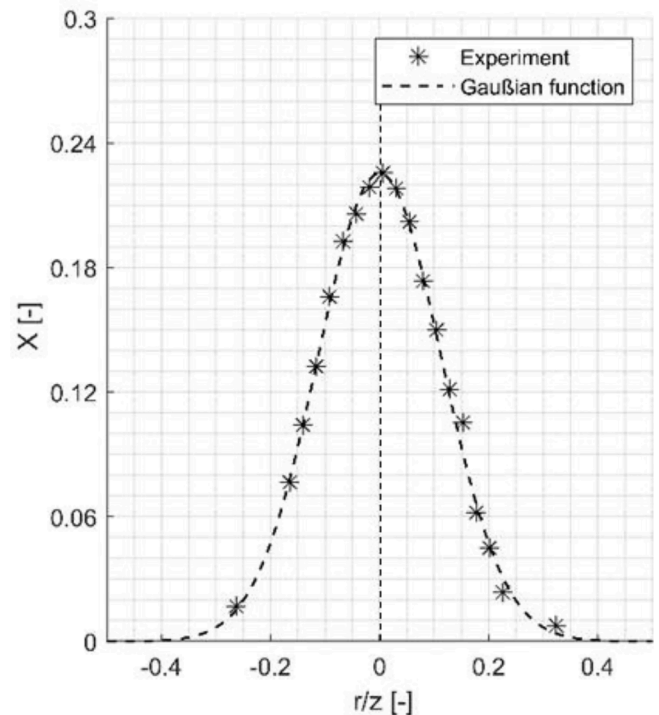
Fig. 3. Radial profile of the mixing ratio X determined from the experiment (nozzle 1, GLR = 0.5, z = 131 mm) and a fitted Gaussian curve.

For single-phase free jets (Fig. 4) and two-phase free jets (Fig. 5), the mixing ratio in the gas phase X at the centerline ($\eta = 0$) are plotted over $\frac{1}{\zeta} = d_{eq}/(z - z_0)$. For each radial profile, $X(\eta = 0)$ is determined using parameter a of the fitted Gaussian curve (see Eq. (10)). In the present study, the value of the virtual jet origin z_0 is chosen to be constant and equal to $z_0 = -3mm$, which is in the range reported in the literature for nozzle 1–3 (see Section 1.2). Thus, the extrapolated lines connecting the measuring points in Fig. 4 and Fig. 5 result in good approximation in straight lines through the origin, the mixing ratio on the centerline is found to decrease inversely-proportionally to ζ for both single-phase and two-phase free jets.

The slope of the straight lines are the values for B_c in Eq. (5). For the single-phase free jet (see Fig. 4), the values for B_c are determined to 5.74 (nozzle 1), 5.67 (nozzle 2) and 4.44 (nozzle 3), which is in the range of $\pm$ 10 % the values reported in literature (4.35 – 5.41) [9,38,40,41,48,50,51].

For the two-phase free jet (see Fig. 5), the liquid mass flow has been varied according to $0.5 \leq GLR \leq 1.5$. No significant influence of the liquid mass flow or the GLR, respectively, on the mixing ratio of the gas phase is found. Therefore, a mean centerline decay rate is calculated from the $5 GLR$ s for each nozzle. The centerline decay rates are equal to 3.82 (nozzle 1), 4.05 (nozzle 2), and 4.44 (nozzle 3).

For nozzle 3 (Fig. 5c), no difference between the single-phase free jet and two-phase free jet in terms of B_c is found. For nozzles 1 (Fig. 5a) and 2 (Fig. 5b), the mixing ratio on the axis of the two-phase free jet decreases faster with increasing axial distance than the mixing ratio of the single-phase free jet. We assume that the atomization process initiates the difference between nozzles 1 and 2 compared to nozzle 3, which is discussed at the end of this section.

In Fig. 6, the local mixing ratios $X(\eta, \zeta)$ of all two-phase measurements conducted are multiplied by the axial distance ζ. The radial profiles measured at different axial distances form a cloud of points, which collapse close to a single line. This phenomenon is known as self-similarity of the free jet [3,5,6], which is common to the single-phase free jet (see Section 1.2). Therefore, self-similarity is also found for the two-phase free jet.

The parameter for the exchange of momentum c_i for the semi-empirical two-phase free jet model, which is presented in [1], is obtained by minimizing the difference in the measured values of X, and X calculated from Eq. (6) using a non-linear least-square solver (see Section 2.3). In order to prove the measuring concept, single phase free jets

from the 3 nozzles are investigated (see Table 1). For each nozzle, one single value for c_i is determined, representing all axial and radial positions. The parameter for exchange of momentum c_i for the single-phase free jet is determined for the 3 nozzles to be equal to 0.0681, 0.0692 and 0.0771, respectively. These values are in good accordance with the literature value ($c_i = 0.07$) [52] for single-phase free jets (see Section1.2).

For the two-phase free jet, c_i is also determined. Following the results given above, no influence of GLR is considered. Thus, for each nozzle, only one single value of c_i is determined (see Fig. 6). The standard deviation between the experimental data and the fitted free jet model is determined for all two-phase free jet measurements conducted to be $\sigma = 0.035$. The standard deviation of the free jet model (Eq. (6)) is one order of magnitude higher compared to that of the Gaussian function (see Fig. 3), as each single radial profile is fitted to the Gaussian function using the 3 parameters $a, b,$ and c, whereas the free jet model (Eq. (6)) only uses a single parameter (c_i) to represent the data measured with each nozzle (5 radial profiles, $5 GLR$ s). However, the low value of $\sigma = 0.035$ shows that the free jet model (Eq. (6)) with fitted values of c_i for each nozzle reproduces the measured values of the mixing ration in the gas phase of the two-phase free jet to a good degree of approximation.

For the single-phase free jet, the parameter for the exchange of momentum, which represents the spreading of the gas jet, is a constant. For two-phase free jets, c_i depends on the nozzle configuration and the operating conditions. The value of c_i for nozzle 3 ($c_i = 0.0776$) is close to the value for a single-phase from the literature ($c_i = 0.07$), whereas the values for nozzles 1 and 2 ($c_i = 0.0856$; $c_i = 0.0870$) differ significantly. In Fig. 5, the same difference between the single-phase and two-phase free jet is apparent in the centerline decay. We assume that the atomization process initiates the difference of c_i for the two-phase experiments with nozzles 1 and 2. In order to investigate this phenomenon, high-speed camera imaging is used to obtain visual information of the atomization process for each nozzle and GLR.

The primary jet breakup can be classified according to the nozzle dimensions and the operating conditions into different atomization regimes. Operating condition of nozzles 1 and 2 lead to the atomization in Fiber-type breakup with pulsating sub-mode. In this sub-mode, the liquid core is moved periodically in radial direction, which causes a radial acceleration of the droplets and a wide spray angle (see Fig. 7) [57,61]. The frequency of the liquid jet's periodic movement was determined for nozzles 1 and 2 to 240 ± 10 Hz from high-speed camera images. The frequency is mainly influenced by the gas velocity at the
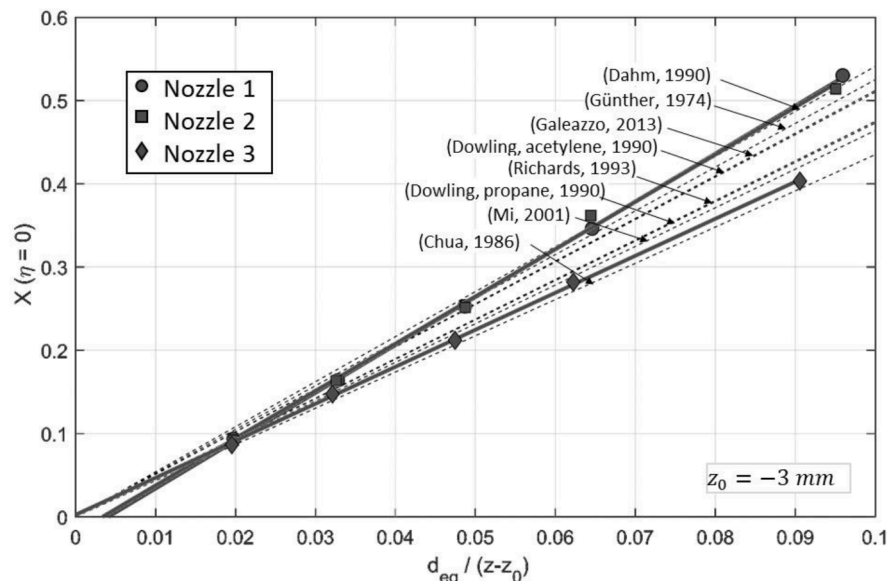
Fig. 4. Mixing ratio on the centerline of the single-phase free jet measured with nozzle 1–3 and from literature [9,38,40,41,48,50,51].
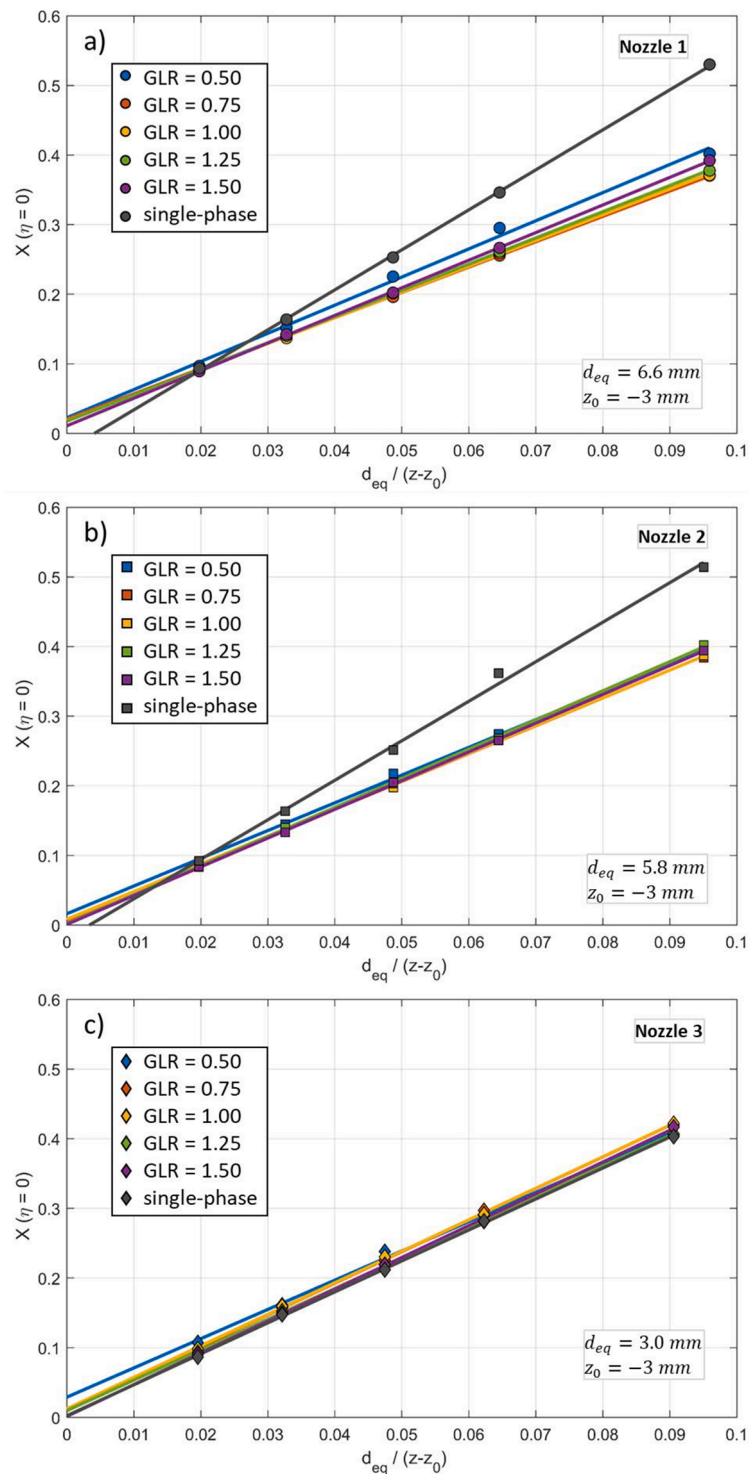
Fig. 5. Comparison of the mixing ratio on the centerline between the single-phase free jet and the gas phase of the two-phase varying *GLR* for a) nozzle 1, b) nozzle 2 and c) nozzle 3.

nozzle orifice, which is 72 m/s for nozzle 1 and 80 m/s for nozzle 2, respectively. The frequency detected is in good accordance to Delon et al. [60] measuring frequencies in the range of 200 – 300 Hz for similar nozzle geometries and gas outlet velocities between 65 and 90 m/s.

The spray angle θ was obtained from measurements of the liquid mass flux using a mechanical patternator [35]. The spray angle was defined as the radial position, where the local mass flux is reduced to 5 % of the liquid mass flux at the center of the spray. The spray angle of nozzles 1 and 2 is determined to approximately 40° and for nozzle 3 to

26°, respectively (see Fig. 7). In the slipstream of the droplets, gas from the center of the free jet is transported in radial direction. Therefore, the radial movement of the droplets may also enhance radial mixing and therefore entrainment of the gas phase, which results in an increase of c_i. Primary breakup of the liquid jet emerging from nozzle 3 is in the Fiber-type regime with super-pulsating sub-mode. In this sub-mode, radial acceleration of the liquid primary jet is not observed. The value of c_i determined in the experiments is close to that of single-phase free jets reported from literature Furthermore, typical droplet diameters for
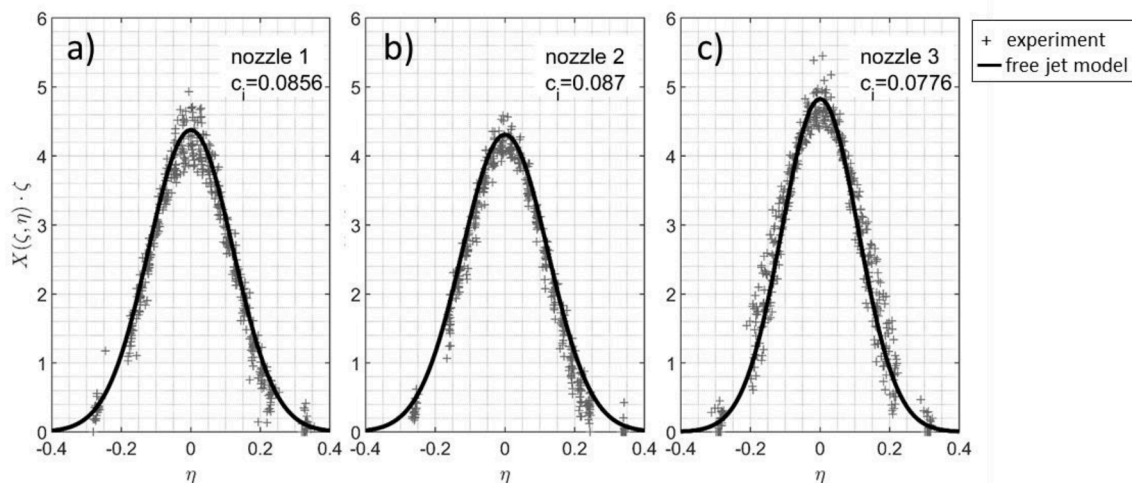
Fig. 6. Measured mixing ratio of the gas phase (all measurements conducted) and free jet model (Eq. (6)) with fitted parameter for the exchange of momentum c_i for the 3 nozzles investigated.
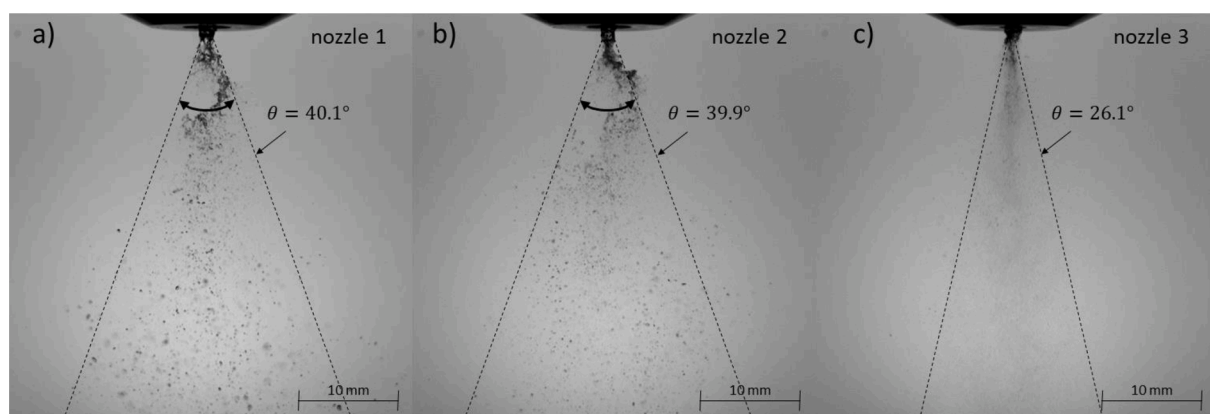
Fig. 7. High speed camera (Photron FastCam SA4) images of the primary jet breakup for nozzle 1 – 3 at GLR = 1.00 and the spray angle θ determined with a mechanical patternator. Nozzle 1 and nozzle 2: Fiber-type pulsating; nozzle 3: Fiber-type super-pulsating. Camera setting are chosen according to [66].

the operating conditions chosen for nozzles 1 and 2 are larger as compared to droplet diameters using operating conditions of nozzle 3. Large droplets enhance turbulence and therefore radial mixing due to the vortex shedding phenomenon [55]. Close to the nozzle, particle size and relative velocity between gas phase and droplet are in the range, where vortex shedding may occur. Typical particle sizes for nozzle 3 are small compared to nozzles 1 and 2. In order to create the droplet surface during the atomization, energy is required, which is provided by the kinetic energy of the atomization medium. However, the kinetic energy provided by the atomization medium is 2–3 orders of magnitude higher than the energy required for the generation of new droplet surface thus has only minor effect. Furthermore, the disperse phase can influence the turbulence structure of the gas phase and therefore the mixing in the gas phase [56].

4. Conclusion

This paper presents measurements of the local mixing ratio in the gas-phase of a two-phase free jet at ambient conditions. The mixing ratio of the gas phase represents entrainment in the gas phase. The mixing ratio is determined at several radial and axial positions for 3 different external-mixing twin-fluid nozzles. In the experiments, water is atomized by pressurized air, which is enriched with helium as a tracer gas. The mixing ratio in the jet is determined by a concentration

measurement of helium. Different gas-to-liquid ratios for the two-phase free jet and a single-phase free jet using only pressurized air are investigated for each nozzle.

Common characteristics between the gas phase in the two-phase free jet and the single-phase free jet have been found. First, the radial profiles of the mixing ratio of two-phase free jet are found to be of Gaussian shape (see Fig. 6). Second, the mixing ratio on the axis of the two-phase free jet is found to decrease inversely-proportionally to the axial distance ζ (seeFigure 5). Third, the two-phase free jet is found to show self-similarity (see Fig. 6). For nozzles operated in the atomization regime with super-pulsating sub-mode, no difference between the mixing ratio of the gas phase in the two-phase free jet and a single-phase free jet has been detected. For operating conditions in the atomization regime with pulsating sub-mode, entrainment in the gas phase of the two-phase free jet is increased compared to the single-phase free jet. The spray angle for both sub-modes has been determined using a mechanical patternator (see Fig. 7). In the pulsating sub-mode, the spray angle is significantly larger than in the super-pulsating sub-mode, which may also enhance entrainment in the gas phase. For quantitative evaluation, further investigations are necessary. For the two-phase free jet, the liquid mass flow has been varied. No further influence of the liquid mass flow on the mixing ratio of the gas phase is found (see Fig. 5).

The experimental data is also used to determine the empirical parameters for the exchange of momentum (c_i) of the two-phase free jet

model for the simulation of the flame structure in an entrained flow gasifier [1]. Measuring data of the mixing ratio is available on Mendeley data as supplementary material of the present research (https://doi.org/10.17632/t66f8swg6w.1) [2].

CRediT authorship contribution statement

Christian Hotz: Conceptualization, Methodology, Investigation, Writing – original draft. **Manuel Haas:** Writing – review & editing. **Simon Wachter:** Writing – review & editing. **Sabine Fleck:** Writing – review & editing. **Thomas Kolb:** Writing – review & editing, Supervision.

Declaration of Competing Interest

The authors declare that they have no known competing financial interests or personal relationships that could have appeared to influence the work reported in this paper.

Acknowledgments

References

[1] Hotz C, Haas M, Wachter S, Fleck S, Kolb T. Two-phase free jet model of an atmospheric entrained flow gasifier. Fuel 2021;304(21–23):121392. https://doi.org/10.1016/j.fuel.2021.121392.

[2] Hotz C. Data for: Experimental investigation on entrainment in two-phase free jets. Mendeley Data 2022. https://doi.org/10.17632/t66f8swg6w.1.

[3] Panchapakesan NR, Lumley JL. Turbulence measurements in axisymmetric jets of air and helium. Part 1. Air jet. J Fluid Mech 1993;246:197–223. https://doi.org/10.1017/S0022112093000096.

[4] Panchapakesan NR, Lumley JL. Turbulence measurements in axisymmetric jets of air and helium. Part 2. Helium jet. J Fluid Mech 1993;246:225–47. https://doi.org/10.1017/S0022112093000102.

[5] Hussein HJ, Capp SP, George WK. Velocity measurements in a high-Reynolds-number, momentum-conserving, axisymmetric, turbulent jet. J Fluid Mech 1994;258(-1):31. https://doi.org/10.1017/S002211209400323X.

[6] Wygnanski I, Fiedler H. Some measurements in the self-preserving jet. J Fluid Mech 1969;38(03):577. https://doi.org/10.1017/S0022112069000358.

[7] Hinze JO. Turbulence. 2nd ed. New York, NY: McGraw-Hill; 1975.

[8] Burattini P, Antonia RA, Danaila L. Similarity in the far field of a turbulent round jet. Phys Fluids 2005;17(2):25101. https://doi.org/10.1063/1.1833414.

[9] Galeazzo FCC. Simulation of Turbulent Flows with and without Combustion with Emphasis on the Impact of Coherent Structures on the Turbulent Mixing [Dissertation]. Karlsruher Institut für Technologie; 2013.

[10] Armenio V, Geurts B, Fröhlich J. Direct and Large-Eddy Simulation VII. Dordrecht: Springer, Netherlands; 2010.

[11] Dimotakis PE. Turbulent mixing. Annu Rev Fluid Mech 2005;37(1):329–56. https://doi.org/10.1146/annurev.fluid.36.050802.122015.

[12] Wachter S, Jakobs T, Kolb T. Towards system pressure scaling of gas assisted coaxial burner nozzles – An empirical model. Applications in Energy and Combustion Science 2021;5:100019. https://doi.org/10.1016/j.jaecs.2020.100019.

[13] Wachter S, Jakobs T, Kolb T. Effect of Solid Particles on Droplet Size Applying the Time-Shift Method for Spray Investigation. Appl Sci 2020;10(21):7615. https://doi.org/10.3390/app10217615.

[14] Hede PD, Bach P, Jensen AD. Two-fluid spray atomisation and pneumatic nozzles for fluid bed coating/agglomeration purposes: A review. Chem Eng Sci 2008;63(14):3821–42. https://doi.org/10.1016/j.ces.2008.04.014.

[15] Lefebvre AH. Twin-fluid atomization: Factors influencing mean droplet size. Atomiz Spr 1992;2(2):101–19. https://doi.org/10.1615/AtomizSpr.v2.i2.30.

[16] Aisa L, Garcia JA, Cerecedo LM, Garcia Palacin I, Calvo E. Particle concentration and local mass flux measurements in two-phase flows with PDA. Application to a study on the dispersion of spherical particles in a turbulent air jet. Int J Multiph Flow 2002;28(2):301–24. https://doi.org/10.1016/S0301-9322(01)00071-4.

[17] Lau TCW, Nathan GJ. Influence of Stokes number on the velocity and concentration distributions in particle-laden jets. J Fluid Mech 2014;757:432–57. https://doi.org/10.1017/jfm.2014.496.

[18] Iqbal N, Rauh C, Delgado A. Numerical Simulations of Particle-laden jet/spout Flows Using Eulerian-Lagrangian Approach. Procedia Eng 2015;102:867–76. https://doi.org/10.1016/j.proeng.2015.01.207.

[19] Horwitz J, Rahmani M, Geraci G, Banko A, Mani A. Two-way coupling effects in Particle-Laden Turbulence: how particletracking scheme affects particle and fluid statistics. ICMF 2016;2016.

[20] Jiang X, Siamas GA, Jagus K, Karayiannis TG. Physical modelling and advanced simulations of gas–liquid two-phase jet flows in atomization and sprays. Prog Energy Combust Sci 2010;36(2):131–67. https://doi.org/10.1016/j.pecs.2009.09.002.

[21] Basu P. Biomass Gasification and Pyrolysis 2010.

[22] Jakobs T, Djordjevic N, Fleck S, Mancini M, Weber R, Kolb T. Gasification of high viscous slurry R&D on atomization and numerical simulation. Appl Energy 2012;93:449–56. https://doi.org/10.1016/j.apenergy.2011.12.026.

[23] Molino A, Larocca V, Chianese S, Musmarra D. Biofuels Production by Biomass Gasification: A Review. Energies 2018;11(4):811. https://doi.org/10.3390/en11040811.

[24] Probstein RF. Synthetic Fuels. Dover Publications; 2013.

[25] Fleck S, Santo U, Hotz C, Jakobs T, Eckel G, Mancini M, et al. Entrained flow gasification Part 1: Gasification of glycol in an atmospheric-pressure experimental rig. Fuel 2018;217:306–19. https://doi.org/10.1016/j.fuel.2017.12.077.

[26] Mancini M, Alberti M, Dammann M, Santo U, Eckel G, Kolb T, et al. Entrained flow gasification. Part 2: Mathematical modeling of the gasifier using RANS method. Fuel 2018;225(4):596–611. https://doi.org/10.1016/j.fuel.2018.03.100.

[27] Becker HA, Hottel HC, Williams GC. Mixing and Flow in ducted turbulent Jets: At Cornell University Ithaca, New York, August 27 to September 1, 1962 1963.

[28] Field MA. Combustion of pulverized coal. Leatherhead (Sy) 1967.

[29] Thring MW, Newby MP. Combustion length of encloed turbulent jet flames. Symp (Int) Combust 1953;4:789–96.

[30] Guruz AG, Guruz HK, Osuwan S, Steward FR. Aerodynamics of a Confined Burning Jet. Combust Sci Technol 1974;9(3–4):103–10. https://doi.org/10.1080/00102207408960344.

[31] Smith MS. The Effect of buoyancy in Enclosed Turbulent Flames [Dissertation]. Surrey: University of Surrey; 1976.

[32] Laats MK. Experimental study of the dynamics of an air-dust jet. Inzhenerno-Fiziche Skii Zhurnal 1966;10:11–5.

[33] Sheen HJ, Jou BH, Lee YT. Effect of particle size on a two-phase turbulent jet. Exp Therm Fluid Sci 1994;8(4):315–27. https://doi.org/10.1016/0894-1777(94)90061-2.

[34] Subramanian V, Ganesh R. Influence of free stream velocity on the entrainment by single- and two-phase axisymmetric jets. AIChE J 1984;30(6):1010–3. https://doi.org/10.1002/aic.690300626.

[35] Schelling J, Reh L. Influence of atomiser design and coaxial gas velocity on gas entrainment into sprays. Chem Eng Process 1999;38(4–6):383–93. https://doi.org/10.1016/S0255-2701(99)00036-7.

[36] Pitts WM. Effects of global density ratio on the centerline mixing behavior of axisymmetric turbulent jets. Exp Fluids 1991;11–11(2–3):125–34. https://doi.org/10.1007/BF00190288.

[37] Pitts WM. Reynolds number effects on the mixing behavior of axisymmetric turbulent jets. Exp Fluids 1991;11–11(2–3):135–41. https://doi.org/10.1007/BF00190289.

[38] Mi J, Nobes DS, Nathan GJ. Influence of jet exit conditions on the passive scalar field of an axisymmetric free jet. J Fluid Mech 2001;432:91–125.

[39] Xu G, Antonia R. Effect of different initial conditions on a turbulent round free jet. Exp Fluids 2002;33(5):677–83. https://doi.org/10.1007/s00348-002-0523-7.

[40] Dowling DR, Dimotakis PE. Similarity of the concentration field of gas-phase turbulent jets. J Fluid Mech 1990;218:109–41.

[41] Richards CD, Pitts WM. Global density effects on the self-preservation behaviour of turbulent jets. J Fluid Mech 1993;254:417–35.

[42] Rotta JC. Turbulente Strömungen: Eine Einführung in die Theorie und ihre Anwendung. Göttingen, Göttingen: Niedersächsische Staats-und Universitätsbibliothek; Univ.-Verl. Göttingen; 2010.

[43] Reichardt H. Gesetzmäßigkeiten der freien Turbulenz. VDI Forschungsheft 1951; 414:2–30.

[44] Corrsin S. Investigation of flow in an axially symmetrical heated jet of air: Investigation of flow in an axially symmetrical heated jet of air. Wartime Report 1943.

[45] Reichardt H. Impuls- und Wärmeaustausch in freier Turbulenz 1944.

[46] Hinze JO, Van Der Hegge Zijnen BG. Transfer of heat and matter in the turbulent mixing zone of an axially symmetrical jet. Appl Sci Res 1949.

[47] Alexander LG, Baron T, Comings EW. Transport of momentum, mass, and heat in turbulent jets. University of Illinois Bulletin Series 1953;413.

[48] Günther R. Verbrennung und Feuerungen. Berlin, Heidelberg: Springer, Berlin Heidelberg; 1974.

[49] Fast G. Laseroptische Strömungsdiagnostik zu Selbstzündungsprozessen bei Freistrahlen [Dissertation]. Eggenstein-Leopoldshafen: Forschungszentrum Karlsruhe; 2007.

[50] Dahm WJA, Dimotakis PE. Mixing at large Schmidt number in the self-similar field of turbulent jets. J Fluid Mech 1990;217:299–330.

[51] Chua LP, Antonia RA. The Turbulent Interaction Region of a Circular Rond Jet. INT. COMM. HEAT MASS TRANSFER 1986.

[52] Kremer H. Zur Ausbreitung inhomogener turbulenter Freistrahlen und turbulenter Diffusionsflammen [Dissertation]. Karlsruhe: Universiät Karlsruhe (TH); 1964.

[53] Crowe CT, Oweis GF, Ceccio SL, Matsumoto Y, Tropea C, Roisman IV. Multiphase Flow Handbook. CRC Press; 2005.

[54] Melville WK, Bray KN. The Two-Phase Turbulent Jet. Int J Heat Mass Transf 1979; 22:279–87.

[55] Hetsroni G. Particles-Turbulence Interaction. Int J Multiph Flow 1989;15:735–46.

[56] Lau TCW, Nathan GJ. The effect of Stokes number on particle velocity and concentration distributions in a well-characterised, turbulent, co-flowing two-phase jet. J Fluid Mech 2016;809:72–110. https://doi.org/10.1017/jfm.2016.666.

[57] Chigier NA, Farago Z, Chigier N. Morphological classification of disintegration of round liquid jets in a coaxial air stream. Atomization Sprays 1992;2(2):137–53. https://doi.org/10.1615/AtomizSpr.v2.i2.50.

[58] Lasheras JC, Hopfinger EJ. Liquid Jet Instability and Atomization in a Coaxial Gas Stream. Annu Rev Fluid Mech 2000;32(1):275–308. https://doi.org/10.1146/annurev.fluid.32.1.275.

[59] Sänger AD. Zerstäubung hochviskoser Fluide bei variierendem Systemdruck - Grundlagenforschung zur Hochdruck-Flugstromvergasung. Dissertation 2018. https://doi.org/10.5445/IR/1000087397.

[60] Delon A, Cartellier A, Matas J-P. Flapping instability of a liquid jet. Phys Rev Fluids 2018;3(4). https://doi.org/10.1103/PhysRevFluids.3.043901.

[61] Matas J-P, Delon A, Cartellier A. Shear instability of an axisymmetric air–water coaxial jet. J Fluid Mech 2018;843:575–600. https://doi.org/10.1017/jfm.2018.167.

[62] Sänger A, Jakobs T, Djordjevic N, Kolb T. Effect of primary instability of a high viscous liquid jet on the spray quality generated by a twin-fluid atomizer. ILASS – Europe 2014, 26th Annual Conference on Liquid Atomization and Spray Systems, 8-10 Sep. 2014, Bremen, Germany 2014.

[63] Coleman TF, Li Y. On the convergence of interior-reflective Newton methods for nonlinear minimization subject to bounds. Math Program 1994;67:189–224.

[64] Coleman TF, Li Y. An Interior Trust Region Approach for Nonlinear Minimization Subject to Bounds. SIAM J Optim 1996;6(2):418–45. https://doi.org/10.1137/0806023.

[65] Warda HA, Kassab SZ, Elshorbagy KA, Elsaadawy EA. An experimental investigation of the near-field region of free turbulent round central and annular jets. Flow Meas Instrum 1999;10(1):1–14. https://doi.org/10.1016/S0955-5986(98)00042-9.

[66] Wachter S, Jakobs T, Kolb T. Experimental investigation on the influence of system pressure on resulting spray quality and jet breakup applying pressure adapted twin-fluid nozzles. Int J Multiph Flow 2020;125:103189. https://doi.org/10.1016/j.ijmultiphaseflow.2019.103189.